Available online at www.eccomasproceedia.org
Eccomas Proceedia COMPDYN (2017) 2910-2925

ECCOMAS
Proceedia

COMPDYN 2017
6th ECCOMAS Thematic Conference on
Computational Methods in Structural Dynamics and Earthquake Engineering
M. Papadrakakis, M. Fragiadakis (eds.)
Rhodes Island, Greece, 15–17 June, 2017

NONSMOOTH MODELLING OF IMPACTS IN ROCKING STRUCTURES WITH POISSON'S LAW

Anastasios I. Giouvanidis[1] **and Elias G. Dimitrakopoulos**[1]

[1]Department of Civil and Environmental Engineering, The Hong Kong University of Science and Technology
Kowloon Bay, Hong Kong
e-mail: agiouvanidis@connect.ust.hk
e-mail: ilias@ust.hk

Keywords: rocking, nonsmooth dynamics, linear complementarity problem, impact, flexible rocking structures, Poisson's contact law.

Abstract. *Rocking action offers a favorable seismic isolation effect that relieves the structure from deformation and damage during strong earthquakes. A complete description of the dynamics of a rocking structure requires, apart from the equation of motion, an appropriate treatment of the contact phenomenon. During rocking, when rotation reverses, the smooth motion of the structure is interrupted by nonsmooth impacts. To date, most analytical and numerical investigations on the rocking behavior treat impacts adopting the 'classical' model of the angular coefficient of restitution or with ad-hoc assumptions. This paper revisits the contact process encountered in two archetypal rocking structures: the rigid rocking block and the flexible rocking oscillator from a nonsmooth dynamics perspective. It considers impact as an instantaneous event and treats it through a system of inequalities known as the linear complementarity problem (LCP). This study models contact behavior with a set-valued Poisson's law in the normal direction and assumes sticking behavior in the tangential direction. The analysis demonstrates the ability of the proposed methodology to capture the impact behavior of different structures rocking on a rigid base. The results show that the proposed LCPs verify corresponding analytical results of other methodologies. Specifically, regarding the rocking block, comparisons of the nonsmooth model with the 'classical' impact model reveal perfect agreement. This study further unveils the substantial role of the Poisson's coefficient of restitution in capturing the experimental response of the flexible rocking oscillator in cases where other analytical models fail. Most importantly, the nonsmooth dynamics approach captures all physically feasible post-impact states, which can be solved both analytically and numerically. Finally, the proposed approach offers a more concise description of the impact problem in rocking structures and it contributes to a more realistic treatment and better understanding of the contact phenomenon during rocking.*

Peer-review under responsibility of the organizing committee of COMPDYN 2017.
doi: 10.7712/120117.5616.17632

1 INTRODUCTION

Rocking action isolates the structure during strong earthquakes (e.g., [27]) and relieves it from deformation and damage. Therefore, rocking motion attracts the attention of many researchers who examine the dynamic behavior of rocking structures either experimentally ([30] and references therein) or analytically ([37, 16, 17, 36, 12, 13, 22, 20, 21, 24, 43] among others). So far, most analytical studies assume rigid planar rocking behavior. Chopra and Yim [9] and Psycharis [35] first examined the dynamics of flexible (deforming) rocking structures. Those studies compared flexible base-fixed structures with structures allowed to uplift, and showed that in most cases base-fixed structures exhibit larger deformations than rocking structures. Recently, studies such as [32, 1, 2, 40, 41, 39, 3, 42, 23, 4, 6] revisited the stability of flexible rocking structures liberating from the small rotations/deformations assumption and considering overturning of the structure.

In general, a complete description of the rocking dynamics requires, apart from the equation of motion, an appropriate treatment of the impact. To date, most analytical studies on the rocking behavior treat impact adopting the 'classical' impact model introduced by Housner [27]. The 'classical' impact model hinges on the conservation of angular momentum and results in a coefficient of restitution which connects the angular velocities before and after the impact (see e.g., [31, 19, 25] among others). However, considering flexible rocking behavior the contact phenomenon becomes more challenging and flexible rocking structures might exhibit a variety of post-impact states [23]. Therefore, more systematic approaches have been proposed in the context of nonsmooth dynamics ([7, 26, 28, 33] and references therein). Such methods rely on either a rigid multibody approach [8, 23], or assume deformable contact points [5], or utilize compliant elements between the contacting bodies [44].

The present study extends [23] and examines the contact behavior of rocking structures from a nonsmooth dynamics perspective adopting Poisson's law. Specifically, it (i) presents the nonsmooth approach to treat sticking (i.e., non-sliding) impacts and (ii) evaluates its implementation to various rocking structures (i.e., rigid block and flexible oscillator).

2 PROPOSED NONSMOOTH APPROACH

2.1 Nonsmooth dynamics

The proposed event-based nonsmooth dynamics approach decomposes the rocking behavior into *smooth motion* and *nonsmooth impacts* [7, 26, 14, 15, 18, 38]. The present study focuses on the impact phenomenon in two archetypal rocking structures (Fig. 2): (i) the rigid block, and (ii) the flexible oscillator. Throughout the study, impact occurs between rigid bodies which cannot overlap (impenetrability constraint) and is considered instantaneous. The analysis assumes that all non-impulsive forces are considered negligible and wave effects within the body are neglected. Further, the deformation the bodies undergoes at the contact points is considered negligible in the body's scale [5]. The focus of the present study is on structures designed to exhibit planar rocking behavior. Hence, sticking (i.e., non-sliding) between contacting bodies is allowed.

2.2 Linear complementarity problem for impact

A linear complementarity problem (LCP) is a set of linear equations in the form of $\mathbf{y} = \mathbf{A}\mathbf{x} + \mathbf{b}$, with matrices $\mathbf{A}$ and $\mathbf{b}$ known, and (to be determined) unknowns non-negative vectors $\mathbf{x} \geq 0$ and $\mathbf{y} \geq 0$ which satisfy the complementarity condition: $\mathbf{y}^T\mathbf{x} = 0$. The LCP

has a wide range of applications in many scientific fields and several algorithmic schemes can solve it numerically (e.g., Lemke's algorithm [29, 11] among others).

The equation of motion for a multibody system with unilateral contacts can be written as:

$$\mathbf{M}\ddot{\mathbf{q}} - \mathbf{h}(\mathbf{C}, \mathbf{K}, \ddot{u}_g(t)) - \mathbf{W}_N\boldsymbol{\lambda}_N - \mathbf{W}_T\boldsymbol{\lambda}_T = \mathbf{0} \tag{1}$$

where $\mathbf{q}$ is the generalized coordinates vector. $\mathbf{M}$, $\mathbf{C}$ and $\mathbf{K}$ are the mass, the damping and the stiffness matrices respectively, and $\mathbf{h}$ is the vector containing all non-impulsive forces e.g., external excitation $\ddot{u}_g(t)$, dissipating and elastic forces. $\mathbf{W}$ are the direction matrices of the contact forces in the normal (subscript '*N*') and the tangential (subscript '*T*') direction of contact. $\boldsymbol{\lambda}$ are the pertinent contact force vectors which are considered positive when they are compressive/repulsive.

Poisson's contact law : Poisson's law divides the impact into two phases, (i) compression and (ii) expansion. The compression phase starts with the initiation of contact at time instant t^- and ends at t^0 when the approaching process of the bodies has been completed. The expansion phase follows, starting at t^0 and finishing at t^+ with the separation of the contacting bodies. Further, Poisson's law defines a coefficient of restitution $\overline{\overline{\varepsilon}}_p$ equal to the ratio of the impulses stored during these two phases: $\boldsymbol{\Lambda}_N^+ = \overline{\overline{\varepsilon}}_p\boldsymbol{\Lambda}_N^0$, where $\overline{\overline{\varepsilon}}_p$ is the diagonal matrix of the Poisson's coefficient of restitution ε_P. To derive the LCPs for the two phases of impact, we integrate the equation of motion (Eq. (1)) once over the time interval of the compression phase (i.e., from t^- to t^0) and once over the time interval of the expansion phase (i.e., from t^0 to t^+) [28].

LCP of the compression phase of impact : Integrating over the time interval of the compression phase Eq. (1) becomes:

$$\dot{\mathbf{q}}^{\mathbf{0}} + \dot{\mathbf{q}}^- = \mathbf{M}^{-1}\mathbf{W}_N\boldsymbol{\Lambda}_N^0 + \mathbf{M}^{-1}\mathbf{W}_T\boldsymbol{\Lambda}_T^0 \tag{2}$$

where vector $\dot{\mathbf{q}}$ denotes the generalized velocities. Pre-multiplying Eq. (2) by $\mathbf{W}_N^T$ (and $\mathbf{W}_T^T$) returns the vectors of the relative contact velocities in the normal $\dot{\mathbf{g}}_N = \mathbf{W}_N^T\dot{\mathbf{q}}$ (and in the tangential $\dot{\mathbf{g}}_T = \mathbf{W}_T^T\dot{\mathbf{q}}$) direction accordingly:

$$\begin{aligned} \dot{\mathbf{g}}_N^0 - \dot{\mathbf{g}}_N^- &= \mathbf{G}_{NN}\boldsymbol{\Lambda}_N^0 + \mathbf{G}_{NT}\boldsymbol{\Lambda}_T^0 \\ \dot{\mathbf{g}}_T^0 - \dot{\mathbf{g}}_T^- &= \mathbf{G}_{TN}\boldsymbol{\Lambda}_N^0 + \mathbf{G}_{TT}\boldsymbol{\Lambda}_T^0 \end{aligned} \tag{3}$$

where the $\mathbf{G}$ matrices are:

$$\begin{aligned} \mathbf{G}_{NN} &= \mathbf{W}_N^T\mathbf{M}^{-1}\mathbf{W}_N, \quad \mathbf{G}_{NT} = \mathbf{W}_N^T\mathbf{M}^{-1}\mathbf{W}_T \\ \mathbf{G}_{TN} &= \mathbf{W}_T^T\mathbf{M}^{-1}\mathbf{W}_N, \quad \mathbf{G}_{TT} = \mathbf{W}_T^T\mathbf{M}^{-1}\mathbf{W}_T \end{aligned} \tag{4}$$

$\boldsymbol{\Lambda}_N^0$, $\boldsymbol{\Lambda}_T^0$ are the impulses in the normal and tangential direction respectively transferred to the body during the compression phase of impact. This study assumes that sliding is prevented. Therefore, the tangential relative (contact) velocity is zero $\dot{\mathbf{g}}_T^0 = \dot{\mathbf{g}}_T^- = \mathbf{0}$ and Eq. (3) gives:

$$\boldsymbol{\Lambda}_T^0 = -\mathbf{G}_{TT}^{-1}\mathbf{G}_{TN}\boldsymbol{\Lambda}_N^0 \tag{5}$$

With the aid of Eq. (5), Eq. (3) yields the LCP for the compression phase of impact

$$\dot{\mathbf{g}}_N^0 = \left(\mathbf{G}_{NN} - \mathbf{G}_{NT}\mathbf{G}_{TT}^{-1}\mathbf{G}_{TN}\right)\boldsymbol{\Lambda}_N^0 + \dot{\mathbf{g}}_N^- \tag{6}$$

with complementarity conditions

$$\dot{\mathbf{g}}_N^0 \geq \mathbf{0}, \;\; \boldsymbol{\Lambda}_N^0 \geq \mathbf{0}, \;\; {\dot{\mathbf{g}}_N^0}^T\boldsymbol{\Lambda}_N^0 = 0 \tag{7}$$

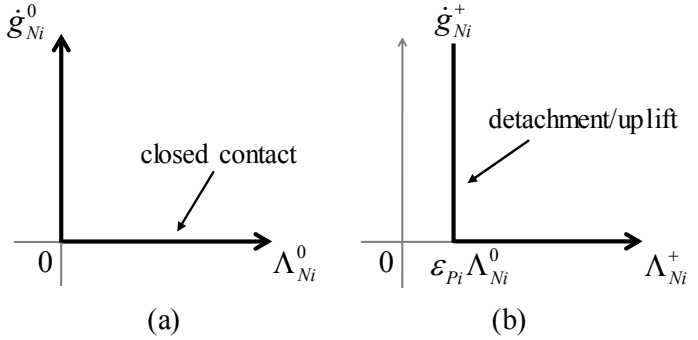

Figure 1: The (unilateral) inequality character of contact. Contact law for (a) the compression and (b) the expansion phase of impact [34].

LCP of the expansion phase of impact : Similarly, integrating Eq. (1) over the time interval of the expansion phase:

$$\dot{\mathbf{q}}^+ + \dot{\mathbf{q}}^0 = \mathbf{M}^{-1}\mathbf{W}_N\mathbf{\Lambda}_{NP} + \mathbf{M}^{-1}\mathbf{W}_N\bar{\bar{\varepsilon}}_p\mathbf{\Lambda}^0_N + \mathbf{M}^{-1}\mathbf{W}_T\mathbf{\Lambda}^+_T \tag{8}$$

and pre-multiplying by $\mathbf{W}^T_N$ and $\mathbf{W}^T_T$:

$$\begin{aligned}\dot{\mathbf{g}}^+_N - \dot{\mathbf{g}}^0_N &= \mathbf{G}_{NN}\mathbf{\Lambda}_{NP} + \mathbf{G}_{NN}\bar{\bar{\varepsilon}}_p\mathbf{\Lambda}^0_N + \mathbf{G}_{NT}\mathbf{\Lambda}^+_T \\ \dot{\mathbf{g}}^+_T - \dot{\mathbf{g}}^0_T &= \mathbf{G}_{TN}\mathbf{\Lambda}_{NP} + \mathbf{G}_{TN}\bar{\bar{\varepsilon}}_p\mathbf{\Lambda}^0_N + \mathbf{G}_{TT}\mathbf{\Lambda}^+_T\end{aligned} \tag{9}$$

Impulse $\mathbf{\Lambda}_{NP} = \mathbf{\Lambda}^+_N - \bar{\bar{\varepsilon}}_p\mathbf{\Lambda}^0_N$ is a modification of the original Poisson's impulse ($\mathbf{\Lambda}^+_N$) which ensures the satisfaction of the impenetrability constraint for multi-point impact problems [28]. Again, assuming zero tangential relative velocity, Eq. (9) gives:

$$\mathbf{\Lambda}^+_T = -\mathbf{G}^{-1}_{TT}\mathbf{G}_{TN}\mathbf{\Lambda}_{NP} - \mathbf{G}^{-1}_{TT}\mathbf{G}_{TN}\bar{\bar{\varepsilon}}_p\mathbf{\Lambda}^0_N \tag{10}$$

and Eq. (9) with the aid of Eq. (10) yields the LCP for the expansion phase of impact

$$\dot{\mathbf{g}}^+_N = \left(\mathbf{G}_{NN} - \mathbf{G}_{NT}\mathbf{G}^{-1}_{TT}\mathbf{G}_{TN}\right)\mathbf{\Lambda}_{NP} + \left(\mathbf{G}_{NN} - \mathbf{G}_{NT}\mathbf{G}^{-1}_{TT}\mathbf{G}_{TN}\right)\bar{\bar{\varepsilon}}_p\mathbf{\Lambda}^0_N + \dot{\mathbf{g}}^0_N \tag{11}$$

with complementarity conditions

$$\dot{\mathbf{g}}^+_N \geq \mathbf{0},\ \ \mathbf{\Lambda}_{NP} \geq \mathbf{0},\ \ \dot{\mathbf{g}}^{+T}_N\mathbf{\Lambda}_{NP} = 0 \tag{12}$$

3 RIGID ROCKING BLOCK USING THE PROPOSED NONSMOOTH APPROACH

The present section revisits the impact behavior of the rigid rocking block of Fig. 2(a) adopting the proposed nonsmooth dynamics approach. Firstly, this study offers closed-form expressions for all the feasible post-impact states solving analytically the proposed LCPs (Eqs (6), (11)). Consider the rigid block of Fig. 2(a) with base-width $2b$ and height $2H$. The generalized coordinates vector for the planar rocking motion of the block is: $\mathbf{q} = \left[\begin{array}{ccc} x & y & \phi \end{array}\right]^T$, where x and y are the translations along the pertinent axes, and ϕ is the planar rocking rotation. Following [14, 15, 18], the two closed contact points (i.e., pivot points '1' and '2') produce two forces/impulses in the normal direction of contact (one force per contact point), but only one force in the tangential direction of contact; the resultant of the two tangential forces at the two pivot points as in Fig. 3. Thus, the mass matrix and the direction matrices in the normal and tangential direction of contact become respectively [23]:

$$\mathbf{M} = \left[\begin{array}{ccc} m & 0 & 0 \\ 0 & m & 0 \\ 0 & 0 & I_G \end{array}\right],\ \mathbf{W}_N = \left[\begin{array}{cc} 0 & 0 \\ 1 & 1 \\ -b & b \end{array}\right],\ \mathbf{W}_T = \left[\begin{array}{c} 1 \\ 0 \\ H \end{array}\right] \tag{13}$$

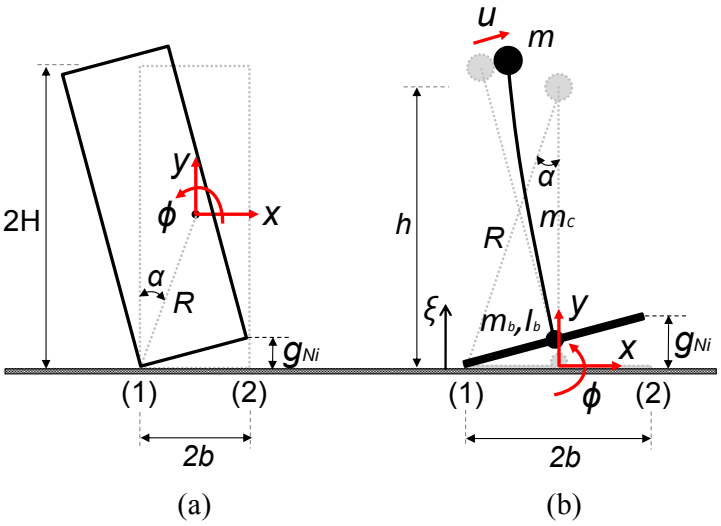

Figure 2: The examined rocking structures: (a) rigid block, (b) flexible oscillator.

where I_G is the mass moment of inertia with respect to the center of mass of the block. For a rectangular block $I_G = (1/3)\, mR^2$, where m is the total mass of the block and R is the half-diagonal distance (Fig. 2(a)).

3.1 Analysis of all physically feasible post-impact states

With reference to Fig. 3, consider a rigid block performing pure rotation (i.e., non-sliding) about pivot point '1' ($g_{N1}^- = \dot{g}_{N1}^- = 0$). Impact takes place at pivot point '2' at the moment $g_{N2}^- = 0$ and with pre-impact contact velocity $\dot{g}_{N2}^- = 2b\dot{\phi}^- < 0$. Note that, negative velocity $\dot{g}_{Ni}$ indicates approach. Fig. 3 illustrates all the physically feasible states during the compression and the expansion phase of impact according to Poisson's law.

3.1.1 Poisson's law - Compression phase

Fig. 3(C) illustrates the potential impact states during the compression phase. The grey color in Fig. 3 indicates the unfeasible impact states.

Bouncing ($A \rightarrow C_1$) (Fig. 3) : The analysis shows that bouncing is not a feasible state during the compression phase of impact according to Poisson's law, since it results to violation of the impenetrability constraint.

Full contact ($A \rightarrow C_2$) (Fig. 3) : Assume that both contact points of the block remain in full contact with the ground during the compression phase of impact. Hence, the normal relative velocities at both contact points are $\dot{g}_{N1}^0 = \dot{g}_{N2}^0 = 0$, and hence known. Therefore, the remaining two unknowns, the two impulses Λ_{N1}^0, Λ_{N2}^0, are both positive because of the complementarity behavior of Eq. (7). The solution of the LCP of Eq. (6) yields:

$$\frac{\Lambda_{N1}^0}{m\dot{g}_{N2}^-} = \frac{1}{3\sin^2\alpha} - \frac{1}{2}, \quad \frac{\Lambda_{N2}^0}{m\dot{g}_{N2}^-} = -\frac{1}{3\sin^2\alpha} \tag{14}$$

with the help of which, Eq. (5) provides the (dimensionless) tangential impulse:

$$\frac{\Lambda_T^0}{m\dot{g}_{N2}^-} = \frac{\cot\alpha}{2} \tag{15}$$

The inequality character of contact determines the (existential) conditions under which each state occurs. Specifically, the $\Lambda_{N1}^0 > 0$ condition of Eq. (7) and Eq. (14) show that the block remains in full contact with the ground when:

$$\frac{H}{b} < \frac{1}{\sqrt{2}} \tag{16}$$

in agreement with [27, 8] using different impact models.

Rocking ($A \rightarrow C_3$) (Fig. 3) : Assume that the block changes pivot point and rocks during the compression phase of impact as Fig. 3(C_3) shows. Hence, contact at point '1' is lost $\dot{g}_{N1}^0 > 0$, while the new contact at point '2' is maintained $\dot{g}_{N2}^0 = 0$. The complementarity conditions (Eq. (7)) return $\Lambda_{N1}^0 = 0$ and $\Lambda_{N2}^0 > 0$. The solution of the LCP of Eq. (6) yields the remaining two unknowns, the normal contact velocity $\dot{g}_{N1}^0$ of point '1' and the normal impulse Λ_{N2}^0 at point '2':

$$\frac{\dot{g}_{N1}^0}{\dot{g}_{N2}^-} = \frac{3\sin^2\alpha}{2} - 1, \quad \frac{\Lambda_{N2}^0}{m\dot{g}_{N2}^-} = \frac{3\sin^2\alpha}{4} - 1 \tag{17}$$

and from Eq. (5), the tangential impulse becomes:

$$\frac{\Lambda_T^0}{m\dot{g}_{N2}^-} = \frac{3}{4}\sin\alpha\cos\alpha \tag{18}$$

Similarly, the inequality character of contact dictates the (existential) conditions of each state. Specifically, the complementary behavior (Eq. 7) requires $\dot{g}_{N1}^0 > 0$. Hence Eq. (17) implies [27, 8]:

$$\frac{H}{b} > \frac{1}{\sqrt{2}} \tag{19}$$

3.1.2 Poisson's law - Expansion phase

Fig. 3(E) illustrates the physically feasible states during the expansion phase of impact. Note that, the expansion phase is a continuation of the compression phase, hence only the valid compression phase states (i.e., full contact C_2 and rocking C_3) are considered. Again, the grey color in Fig. 3 indicates the unfeasible states.

Rocking ($A \rightarrow C_2 \rightarrow E_2$) (Fig. 3) : The analysis shows that rocking during the expansion phase after full contact in the compression phase is not a feasible state, since the results contradict the impenetrability constraint.

Bouncing ($A \rightarrow C_2 \rightarrow E_1$) (Fig. 3) : After the full contact state during the compression phase of impact, point '1' remains in contact with the ground ($\dot{g}_{N1}^+ = 0$), while contact at point

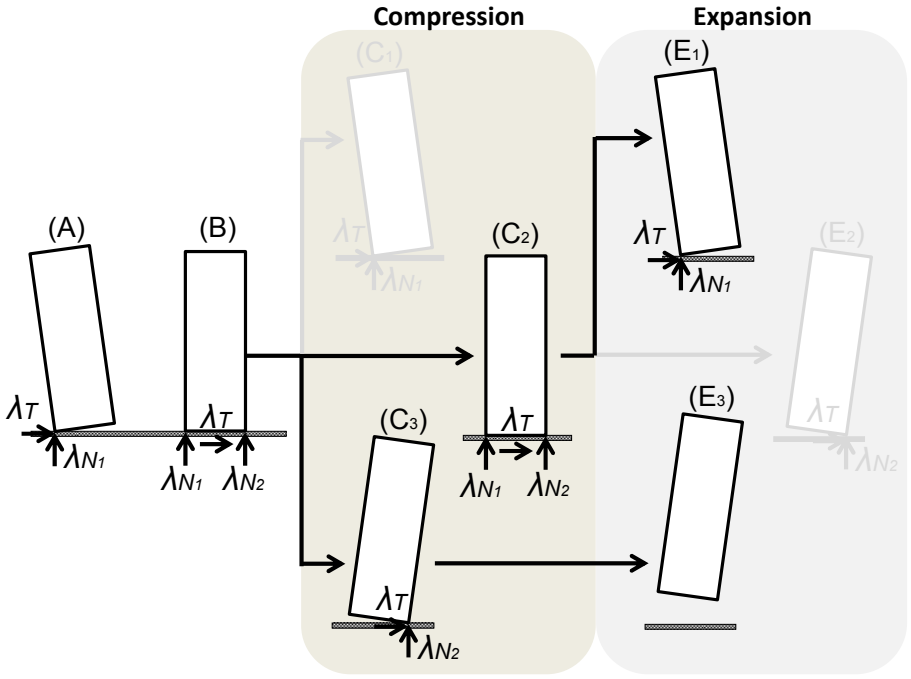

Figure 3: Impact states during the compression (C) and the expansion phase (E) of the rocking block according to Poisson's law.

'2' is lost ($\dot{g}_{N2}^{+} > 0$). Hence, the complementarity conditions of Eq. (12) imply $\Lambda_{NP1} > 0$ and $\Lambda_{NP2} = 0 \Leftrightarrow \Lambda_{N2}^{+} = \varepsilon_p \Lambda_{N2}^{0}$, where Λ_{N2}^{0} is given by Eq. (14). The solution of Eq. (11) gives:

$$\frac{\dot{g}_{N2}^{+}}{\dot{g}_{N2}^{-}} = -\varepsilon_p, \quad \frac{\Lambda_{N1}^{+}}{m\dot{g}_{N2}^{-}} = \varepsilon_p \left(\frac{1}{3\sin^2\alpha} - \frac{1}{2} \right) \tag{20}$$

Therefore, the tangential impulse becomes (Eq. (10)):

$$\frac{\Lambda_{T}^{+}}{m\dot{g}_{N2}^{-}} = \varepsilon_P \frac{\cot\alpha}{2} \tag{21}$$

The (unilateral) inequality character of contact returns the existential conditions for this state to occur. In particular, the complementarity behavior of Eq. (12) and Eq. (20) imply that bouncing becomes feasible when $H/b < 1/\sqrt{2}$; in accordance with Eq. 16.

Flight ($A \rightarrow C_3 \rightarrow E_3$) (Fig. 3) : Point '1' has already lost contact with the ground during the compression phase of impact ($\dot{g}_{N1}^{+} > 0$). Assume that contact at point '2' is also lost at the expansion phase of impact ($\dot{g}_{N2}^{+} > 0$). The complementarity behavior of Eq. (12) yields: $\Lambda_{NP1} = 0 \Leftrightarrow \Lambda_{N1}^{+} = \varepsilon_p \Lambda_{N1}^{0} = 0$ (where $\Lambda_{N1}^{0} = 0$ during the compression phase of impact) and $\Lambda_{NP2} = 0 \Leftrightarrow \Lambda_{N2}^{+} = \varepsilon_p \Lambda_{N2}^{0}$, where Eq. (17) gives Λ_{N2}^{0}. The solution of the LCP of Eq. (11) returns the two unknown relative contact velocities $\dot{g}_{N1}^{+}, \dot{g}_{N2}^{+}$.

$$\frac{\dot{g}_{N2}^{+}}{\dot{g}_{N2}^{-}} = -\varepsilon_p, \quad \frac{\dot{g}_{N1}^{+}}{\dot{g}_{N2}^{-}} = (1+\varepsilon_p) \left(\frac{3\sin^2\alpha}{2} - 1 \right) \tag{22}$$

Eq.(10) yields:

$$\frac{\Lambda_{T}^{+}}{m\dot{g}_{N2}^{-}} = \frac{3}{4}\varepsilon_p \sin\alpha\cos\alpha \tag{23}$$

Similarly, the complementarity behavior of Eq. (12) provides the existential conditions of this state. Specifically, 'flight' becomes a feasible state during the expansion phase of impact only after the rocking state during the compression phase and when $H/b > 1/\sqrt{2}$; in total agreement with Eq. (19).

3.2 Comparison with different impact models/approaches

Eqs (14) to (23) describe completely all possible impact states for the rigid rocking block according to Poisson's contact law. Eqs (14) to (23) prove that the proposed methodology verifies corresponding results from other methodologies, while, at the same time, it encapsulates all physically feasible post-impact states. Specifically, the geometric slenderness criterion derived by [27, 8] is in agreement with Eqs (16), (19). For non-sliding (sticking) impacts, a rocking block is considered 'stocky' when Eq. (16) is satisfied, whereas when Eq. (19) holds the block is regarded as 'slender'.

In many studies, (see e.g., [16, 13, 19, 25] among others), the ratio $\eta = \dot{\phi}^+/\dot{\phi}^-$ defines a coefficient of restitution with respect to the angular velocities before and after the impact. When a (slender) block rocks and 'flights' from the ground during the compression and the expansion phase of impact respectively (Fig. 3(C_3/E_3)), Eqs (2), (8) with the aid of Eqs (17), (18), (22) and (23) yield the relationship between pre- and post-impact angular velocities:

$$\eta = \frac{\dot{\phi}^+}{\dot{\phi}^-} = 1 - \frac{3}{2}\sin^2\alpha - \frac{3}{2}\varepsilon_P \sin^2\alpha \tag{24}$$

Assuming impact is perfectly inelastic (plastic) ($\varepsilon_P = 0$), the impact process terminates at the end of the compression phase and the block exhibits pure rocking behavior (Fig. 3(C_3)). In that case, Eq. (24) agrees with the Housner's angular coefficient of restitution [27].

Eqs (14), (15), 20) and (21) treat the full contact and the bouncing behavior of the block (Fig. 3(C_2/E_1)), with the help of which Eqs (2), (8) give:

$$\eta = \frac{\dot{\phi}^+}{\dot{\phi}^-} = -\varepsilon_p \tag{25}$$

Eq. (25) shows that for $\varepsilon_P = 0$ the block remains in full contact with the ground ($\dot{\phi}^+/\dot{\phi}^- = 0$) and the impact terminates at the end of the compression phase (Fig. 3(C_2)). For perfectly elastic impacts though ($\varepsilon_P = 1$), impulse is transferred to the structure from the compression phase and the block bounces during the expansion phase without any loss of kinetic energy (Fig. 3(E_1)).

3.3 Numerical evaluation of the proposed approach for the rocking block

This section illustrates the versatility of the proposed approach by numerically investigating the response of the rigid rocking block of Fig. 2(a). Following [23], consider (i) a stocky block with $2b$ = 1 m base-width and $H/b = 0.7$ and (ii) a slender block with the same base but $H/b = 7$ (Fig. 2(a)). Fig. 4 illustrates the free rocking response of both structures. Both blocks have the same initial rotation $\phi_0/\alpha = 1/3$, where α is the slenderness of the block. Fig. 4(left) plots the response of the stocky block for three different values of the Poisson's coefficient of restitution and unveils their influence on the response. In particular, the values of the Poisson's coefficient ε_P in Fig. 4(left) simulate different impact conditions. When the impact is considered perfectly inelastic ($\varepsilon_P = 0$), a stocky block stays in full contact with the ground and the impact terminates at the end of the compression phase. However, for perfectly

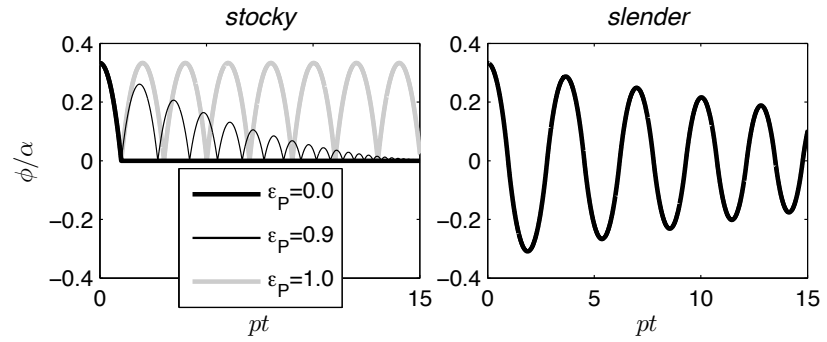

Figure 4: Free rocking response of a stocky ($H/b = 0.7$) and a slender block ($H/b = 7$) starting from the same initial rotation $\phi_0/\alpha = 1/3$ using the proposed nonsmooth approach.

elastic impacts ($\varepsilon_P = 1$) a stocky block bounces without any loss of kinetic energy at every impact; in accordance with the findings of Section 3.2. On the contrary, a slender block, starting from the same initial conditions, changes pivot point and exhibits pure rocking motion for $\varepsilon_P = 0$ (Fig. 4(right)). Note that, all feasible states i.e., full contact, bouncing and pure rocking are captured and solved analytically with the aid of the proposed LCPs of Eqs (6), (11) (Section 3.1).

Fig. 5 assumes that the rocking block starts from rest position under the presence of a ground excitation. Fig. 5 compares the response of the slender rocking block using the proposed nonsmooth approach ($\varepsilon_P = 0$) with the pertinent response using the 'classical' Housner's impact model [27]. The two (identical) blocks exhibit pure rocking motion when subjected to the same sinusoidal pulse with $\alpha_g/g = 0.45$ and $\omega_g/p = 5.75$, where $p = \sqrt{3g/4R}$ is the frequency parameter of the block. g is the gravitational acceleration and R is the half-diagonal length (Fig. 2(a)). Fig. 5 shows that the response of the proposed methodology is in total agreement with the pertinent response of the 'classical' impact model. However, note that, the nonsmooth approach encapsulates all physically feasible post-impact states (i.e., bouncing, flight); something that is not feasible with the 'classical' model.

4 FLEXIBLE ROCKING OSCILLATOR USING THE PROPOSED NONSMOOTH APPROACH

This section investigates the impact phenomenon during the rocking motion of the flexible oscillator of Fig. 2(b) when adopting the proposed nonsmooth dynamics approach. Consider the flexible rocking oscillator of Fig. 2(b) with a lumped mass m at height h, a deformable column with total mass m_c uniformly distributed along its length and a rigid base with mass m_b and width $2b$. Note that, the height of the base is considered negligible compared to its width. The slenderness α of the structure is defined as $\alpha = \operatorname{atan}(b/h)$ (Fig. 2(b)). Assume the concentrated lumped mass m has zero moment of inertia, while the base mass m_b gives moment of inertia $I_b = (1/3)\, m_b b^2$ with respect to its center of mass. The generalized coordinates vector for the planar rocking motion of the flexible rocking oscillator is: $\mathbf{q} = \begin{bmatrix} u & x & y & \phi \end{bmatrix}^T$, where x and y are the translations of the base mass along the pertinent axes, u is the horizontal flexural translation of the lumped mass and ϕ is the planar rocking rotation (Fig. 2(b)). With reference to Fig. 2(b), assume the polynomial shape function of

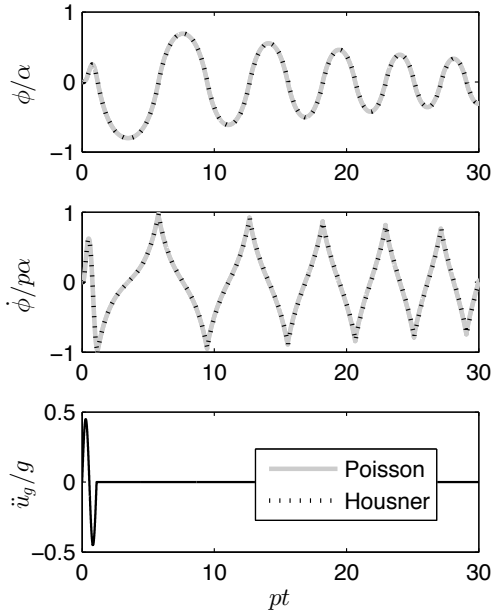

Figure 5: Comparison between the proposed nonsmooth dynamics approach (Poisson's contact law with $\varepsilon_P = 0$) and the 'classical' Housner's impact model [27] for a (slender) rocking block subjected to a sinusoidal pulse with $\alpha_g/g = 0.45$ and $\omega_g/p = 5.75$.

Eq. (26) to describe the deformation of the column [10].

$$\psi(\xi) = \alpha_3 \frac{\xi^3}{h^3} + \alpha_2 \frac{\xi^2}{h^2} + \alpha_1 \frac{\xi}{h} + \alpha_0 \tag{26}$$

where ξ is the distance measured from the base of the column (Fig. 2(b)) and α_0, α_1, α_2, α_3 are constant coefficients. Therefore, the deformation of the column at any arbitrary point is defined as: $u_\xi(\xi, t) = u(t)\,\psi(\xi)$, where $u(t)$ is the generalized coordinate which stands for the flexural translation of the lumped mass.

Before rocking initiates, the oscillator behaves as a single degree of freedom system with generalized mass and stiffness respectively [23]:

$$\begin{aligned} \tilde{m} &= m + \int_0^h \frac{m_c}{h}(\psi(\xi))^2 d\xi = m + \left(\begin{array}{l} \frac{\alpha_3^2}{7} + \frac{\alpha_3\alpha_2}{3} + \frac{2\alpha_3\alpha_1}{5} + \frac{\alpha_3\alpha_0}{2} + \frac{\alpha_2^2}{5} \\ + \frac{\alpha_2\alpha_1}{2} + \frac{2\alpha_2\alpha_0}{3} + \frac{\alpha_1^2}{3} + \alpha_1\alpha_0 + \alpha_0^2 \end{array} \right) m_c \\ \tilde{k} &= \int_0^h EI(\psi''(\xi))^2 d\xi = \tfrac{4EI}{h^3}\left(3\alpha_3^2 + \alpha_2^2 + 3\alpha_3\alpha_2\right) \end{aligned} \tag{27}$$

Following [23], rocking initiates when:

$$\left(\begin{array}{l} \frac{h}{b}\frac{\left(1+\frac{11}{40}\gamma_{m_c}\right)}{\left(1+\frac{33}{140}\gamma_{m_c}\right)} \left(\frac{2\zeta\sqrt{\tilde{m}\tilde{k}}}{mg}\dot{u} + \frac{\tilde{k}}{mg}u + \left(1+\frac{3}{8}\gamma_{m_c}\right)\frac{\ddot{u}_g(t)}{g} \right) \\ -\left(1+\gamma_{m_b}+\gamma_{m_c}\right) - \frac{h}{b}\left(1+\frac{1}{2}\gamma_{m_c}\right)\frac{\ddot{u}_g(t)}{g} + \left(1+\frac{3}{8}\gamma_{m_c}\right)\frac{u}{b} \end{array} \right) \geq 0 \tag{28}$$

where $\gamma_{m_c} = m_c/m$ and $\gamma_{m_b} = m_b/m$. ζ is the damping ratio responsible for the energy dissipation while the structure vibrates. Assuming $\zeta = 0$, $\omega_n = \sqrt{\tilde{k}/\tilde{m}}$ and quasi-static

conditions, Eq. (28) yields the 'critical' (horizontal) flexural translation (u_{cr}) of the lumped mass m necessary to initiate rocking [23].

$$u_{cr} = \frac{\left(1+\gamma_{m_b}+\gamma_{m_c}\right) bg}{\left(1+\frac{11}{40}\gamma_{m_c}\right) h\omega_n^2 + \left(1+\frac{3}{8}\gamma_{m_c}\right) g} \tag{29}$$

After the initiation of rocking, the equations which describe the motion of the flexible rocking oscillator can be derived using the general form of the Lagrange's equation:

$$\frac{d}{dt}\left(\frac{\partial L}{\partial \dot{\phi}}\right) - \frac{\partial L}{\partial \phi} = Q \tag{30}$$

$L = T - V$, where T is the kinetic energy, V is the potential energy and Q is the generalized force. Hence, the equations of motion of the flexible rocking oscillator become [23]:

$$\begin{cases}
\tilde{m}\ddot{u} + \left(m + \left(\frac{\alpha_3}{4}+\frac{\alpha_2}{3}+\frac{\alpha_1}{2}+\alpha_0\right) m_c\right)\cos\phi\ddot{x} + \left(m + \left(\frac{\alpha_3}{4}+\frac{\alpha_2}{3}+\frac{\alpha_1}{2}+\alpha_0\right) m_c\right)\sin\phi\ddot{y} \\
- \left(m + \left(\frac{\alpha_3}{5}+\frac{\alpha_2}{4}+\frac{\alpha_1}{3}+\frac{\alpha_0}{2}\right) m_c\right) h\ddot{\phi} = \\
-2\zeta\sqrt{\tilde{m}\tilde{k}}\dot{u} - \tilde{k}u + \tilde{m}u\dot{\phi}^2 - \left(m + \left(\frac{\alpha_3}{4}+\frac{\alpha_2}{3}+\frac{\alpha_1}{2}+\alpha_0\right) m_c\right)\cos\phi\ddot{u}_g \\
- \left(m + \left(\frac{\alpha_3}{4}+\frac{\alpha_2}{3}+\frac{\alpha_1}{2}+\alpha_0\right) m_c\right)\sin\phi g \\
\\
\left(m + \left(\frac{\alpha_3}{4}+\frac{\alpha_2}{3}+\frac{\alpha_1}{2}+\alpha_0\right) m_c\right)\cos\phi\ddot{u} + \left(m + m_b + m_c\right)\ddot{x} \\
- \left(mh\cos\phi + mu\sin\phi + \frac{1}{2}m_c h\cos\phi + \left(\frac{\alpha_3}{4}+\frac{\alpha_2}{3}+\frac{\alpha_1}{2}+\alpha_0\right) m_c u\sin\phi\right)\ddot{\phi} = \\
- \left(mh\sin\phi - mu\cos\phi + \frac{1}{2}m_c h\sin\phi - \left(\frac{\alpha_3}{4}+\frac{\alpha_2}{3}+\frac{\alpha_1}{2}+\alpha_0\right) m_c u\cos\phi\right)\dot{\phi}^2 \\
+2\left(m + \left(\frac{\alpha_3}{4}+\frac{\alpha_2}{3}+\frac{\alpha_1}{2}+\alpha_0\right) m_c\right)\sin\phi\dot{u}\dot{\phi} - \left(m + m_b + m_c\right)\ddot{u}_g \\
\\
\left(m + \left(\frac{\alpha_3}{4}+\frac{\alpha_2}{3}+\frac{\alpha_1}{2}+\alpha_0\right) m_c\right)\sin\phi\ddot{u} + \left(m + m_b + m_c\right)\ddot{y} \\
+ \left(-mh\sin\phi + mu\cos\phi - \frac{1}{2}m_c h\sin\phi + \left(\frac{\alpha_3}{4}+\frac{\alpha_2}{3}+\frac{\alpha_1}{2}+\alpha_0\right) m_c u\cos\phi\right)\ddot{\phi} = \\
\left(mh\cos\phi + mu\sin\phi + \frac{1}{2}m_c h\cos\phi + \left(\frac{\alpha_3}{4}+\frac{\alpha_2}{3}+\frac{\alpha_1}{2}+\alpha_0\right) m_c u\sin\phi\right)\dot{\phi}^2 \\
-2\left(m + \left(\frac{\alpha_3}{4}+\frac{\alpha_2}{3}+\frac{\alpha_1}{2}+\alpha_0\right) m_c\right)\cos\phi\dot{u}\dot{\phi} - \left(m + m_b + m_c\right) g \\
\\
- \left(m + \left(\frac{\alpha_3}{5}+\frac{\alpha_2}{4}+\frac{\alpha_1}{3}+\frac{\alpha_0}{2}\right) m_c\right) h\ddot{u} - \left(\begin{array}{l} mh\cos\phi + mu\sin\phi + \frac{1}{2}m_c h\cos\phi \\ + \left(\frac{\alpha_3}{4}+\frac{\alpha_2}{3}+\frac{\alpha_1}{2}+\alpha_0\right) m_c u\sin\phi \end{array}\right)\ddot{x} \\
+ \left(-mh\sin\phi + mu\cos\phi - \frac{1}{2}m_c h\sin\phi + \left(\frac{\alpha_3}{4}+\frac{\alpha_2}{3}+\frac{\alpha_1}{2}+\alpha_0\right) m_c u\cos\phi\right)\ddot{y} \\
+ \left(I_{m_b} + mh^2 + \frac{1}{3}m_c h^2 + \tilde{m}u^2\right)\ddot{\phi} = \\
-2\tilde{m}u\dot{u}\dot{\phi} + \left(mh\cos\phi + mu\sin\phi + \frac{1}{2}m_c h\cos\phi + \left(\frac{\alpha_3}{4}+\frac{\alpha_2}{3}+\frac{\alpha_1}{2}+\alpha_0\right) m_c u\sin\phi\right)\ddot{u}_g \\
- \left(-mh\sin\phi + mu\cos\phi - \frac{1}{2}m_c h\sin\phi + \left(\frac{\alpha_3}{4}+\frac{\alpha_2}{3}+\frac{\alpha_1}{2}+\alpha_0\right) m_c u\cos\phi\right) g
\end{cases} \tag{31}$$

For simplicity, the remaining part of the present section adopts $\alpha_0 = \alpha_1 = 0$, $\alpha_2 = 3/2$ and $\alpha_3 = -1/2$ [10]. Further, all the properties of the oscillator and the adopted ground excitations are summarized in [23].

4.1 Numerical evaluation of the proposed approach for the rocking oscillator

This section focuses on the response-history evaluation of the flexible rocking oscillator of Fig. 2(b). Specifically, Fig. 6 compares the response of the oscillator using the proposed nonsmooth approach with the pertinent analytical response (abbreviated as 'VVEL') from [41] and the experimental response from [39] when subjected to the same Ricker pulses. Fig. 6 shows that the proposed nonsmooth model captures very well the experimental response. Further, Fig. 6 unveils the effect of the column elasticity on the response; the stiffer the column, the

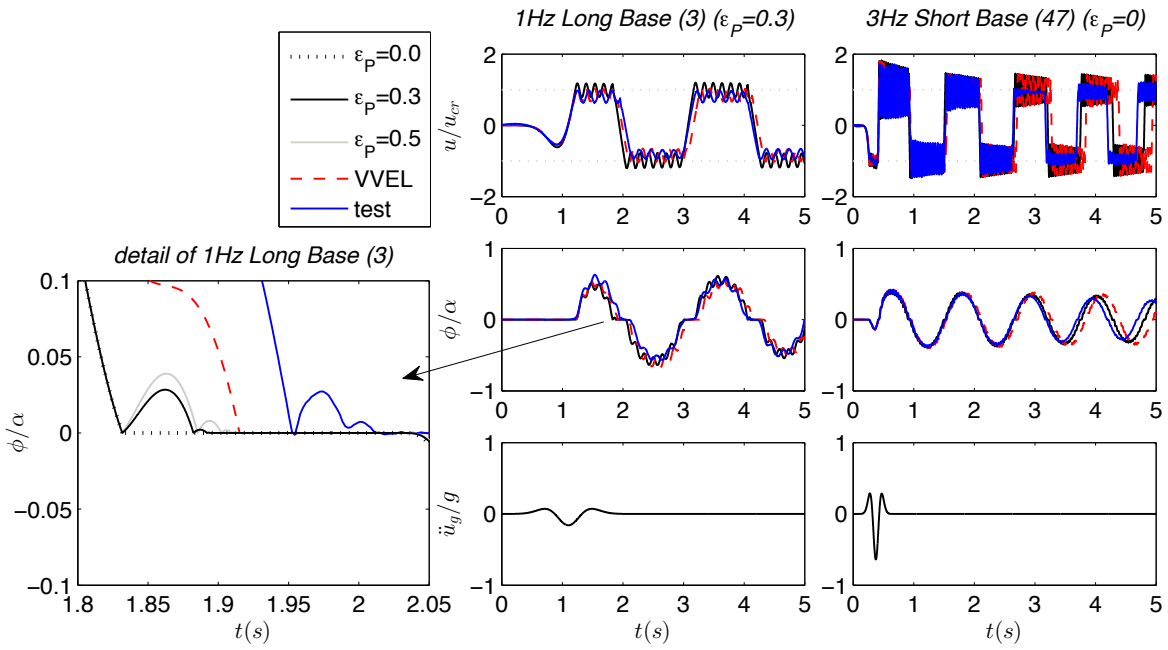

Figure 6: Response-history comparison of the nonsmooth approach with analytical ('VVEL') [41] and experimental results ('test') [39] of the rocking oscillator of Fig. 2(b) when subjected to different Ricker pulses reported in [23] with $\alpha_g/g = 0.16$, $\omega_g/p = 1.95$ (middle) and $\alpha_g/g = 0.64$, $\omega_g/p = 7.73$ (right) accordingly. The nonsmooth response is plotted with an opposite sense to match the assumed positive clockwise rotation in [39, 41].

smoother the rocking motion. A distinct advantage of the proposed nonsmooth model is that it encapsulates all physically feasible post-impact states, with the same mathematical formulation (i.e., the LCPs of Eqs (6), (11)). Fig. 6 reveals that for $\varepsilon_P > 0$ the proposed model predicts bouncing behavior; in agreement with the experimentally observed response. The insert of Fig. 6 illustrates the influence of the Poisson's coefficient of restitution on the response. Note that, the bouncing behavior is more pronounced the more flexible the structure is (i.e., the '1Hz Long Base' compared to the '3Hz Short Base' specimen). Therefore, the stiffer the structure, the smaller the value of the Poisson's coefficient of restitution required to capture the experimental response of the oscillator (Fig. 6).

Fig. 7 compares the response-histories of the rocking oscillator when subjected to historic earthquake records. For consistency, Fig. 7 uses the same values of the Poisson's coefficient of restitution as in Fig. 6. Fig. 7 shows that both analytical models (nonsmooth and 'VVEL') capture well the maximum response of the '1Hz Long Base' specimen. However, after the first rotation cycle the nonsmooth model underestimates the response while the 'VVEL' overestimates it. This underestimation of the response might be caused because of the adopted value of the damping constant ζ presented in [41, 23], or the value of the Poisson's coefficient of restitution ε_P. Recall that, depending on the value of the Poisson's coefficient different amount of energy is dissipated at each impact. The appropriate value is hard to define and merits further investigation. However, this is beyond the scope of the present study. Note that, this is not the case for the '3Hz Short Base' specimen, which the nonsmooth model satisfactorily captures the experimental response.

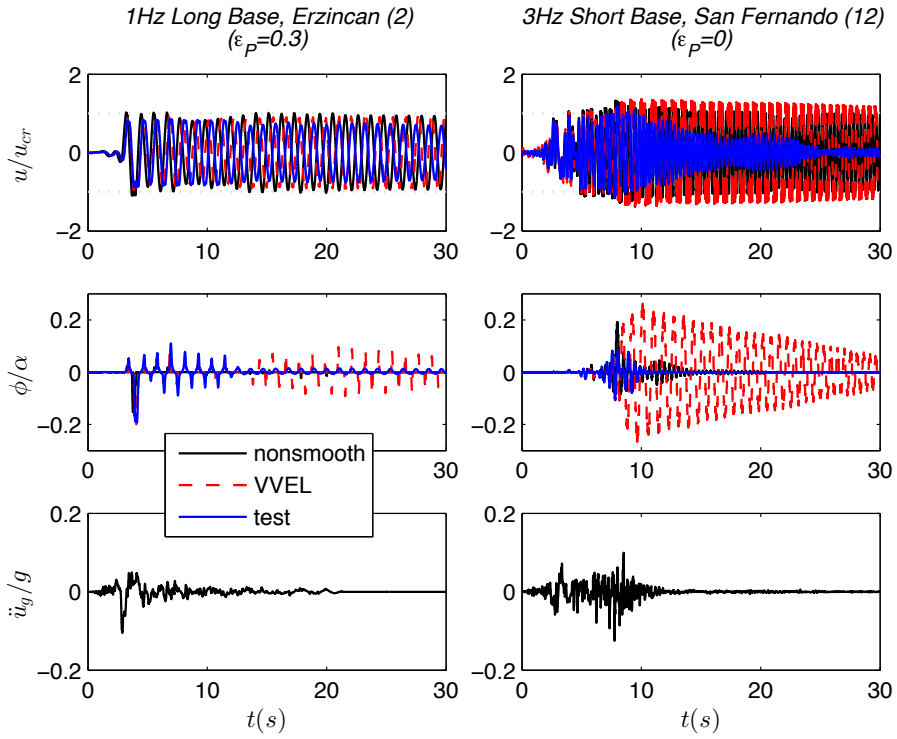

Figure 7: Response-history comparison of the nonsmooth approach with analytical ('VVEL') [41] and experimental results ('test') [39] of the rocking oscillator of Fig. 2(b) when subjected to historic earthquake records reported in [23]. The nonsmooth response is plotted with an opposite sense to match the assumed positive clockwise rotation in [39, 41].

5 CONCLUSIONS

The present study revisits the contact phenomenon encountered in rocking structures adopting a nonsmooth dynamics approach. Two archetypal rocking structures are considered: the rigid rocking block and the flexible rocking oscillator. Throughout the study, impact is considered to be instantaneous. Poisson's law models the behavior in the normal direction of the unilateral contact and sticking behavior is assumed in the tangential direction. This study formulates the impact problem as a system of inequalities, known as the linear complementarity problem (LCP). The proposed LCPs encapsulate all physically feasible post-impact states and liberate from the need for additional ad-hoc assumptions. The analysis shows that, for the case of the rocking block, the closed-form solutions are in total agreement with the pertinent analytical results of other methodologies. Further, the proposed response-history analysis of the flexible rocking oscillator is also validated with numerical and experimental results from literature. Specifically, the analysis shows that with the aid of the Poisson's coefficient of restitution the nonsmooth model captures the complex post-impact experimental response in a way that other analytical models fail. Overall, this work demonstrates the ability of the proposed nonsmooth dynamics approach to capture all physically feasible post-impact states and paves the way for further systematic treatment of the contact phenomenon during rocking.

REFERENCES

[1] Acikgoz, S., DeJong, M. J., The interaction of elasticity and rocking in flexible structures allowed to uplift. *Earthquake Engineering & Structural Dynamics*, **41**(15), 2177–2194, 2012.

[2] Acikgoz, S., DeJong, M. J., The rocking response of large flexible structures to earthquakes. *Bulletin of Earthquake Engineering*, **12**(2), 875–908, 2014.

[3] Acikgoz, S., DeJong, M. J., Analytical modelling of multi-mass flexible rocking structures. *Earthquake Engineering & Structural Dynamics*, **45**(13), 2103-2122, 2016.

[4] Acikgoz, S., DeJong, M. J., Vibration modes and equivalent models for flexible rocking structures. *Bulletin of Earthquake Engineering*, **doi:10.1007/s10518-017-0128-4**, 2017.

[5] Andreaus, U., Casini, P., Dynamics of three-block assemblies with unilateral deformable contacts. Part 1: contact modelling. *Earthquake Engineering & Structural Dynamics*, **28**(12), 1621–1636, 1999.

[6] Avgenakis, E., Psycharis, I. N., Modeling of rocking elastic flexible bodies under static loading considering the nonlinear stress distribution at their base. *Journal of Structural Engineering*, **doi:10.1061/(ASCE)ST.1943-541X.0001783**, 2017.

[7] Brogliato, B., *Nonsmooth mechanics: models, dynamics and control*. Springer, 1999.

[8] Brogliato, B., Zhang, H., Liu, C., Analysis of a generalized kinematic impact law for multibody-multicontact systems, with application to the planar rocking block and chains of balls. *Multibody System Dynamics*, **27**(3), 351–382, 2012.

[9] Chopra, A. K., Yim, S. C. S., Simplified earthquake analysis of structures with foundation uplift. *Journal of Structural Engineering*, **111**(4), 906–930, 1985.

[10] Chopra, A. K., *Dynamics of structures, vol. 4*. Prentice Hall, 1995.

[11] Cottle, R. W., Dantzig, G. B., Complementary pivot theory of mathematical programming. *Linear algebra and its applications*, **1**(1), 103–125, 1968.

[12] DeJong, M. J., Amplification of rocking due to horizontal ground motion. *Earthquake Spectra*, **28**(4), 1405–1421, 2012.

[13] DeJong, M. J., Dimitrakopoulos, E. G., Dynamically equivalent rocking structures. *Earthquake Engineering & Structural Dynamics*, **43**(10), 1543–1563, 2014.

[14] Dimitrakopoulos, E. G., Analysis of a frictional oblique impact observed in skew bridges. *Nonlinear Dynamics*, **60**(4), 575–595, 2010.

[15] Dimitrakopoulos, E. G., Seismic response analysis of skew bridges with pounding deck-abutment joints. *Engineering Structures*, **33**(3), 813–826, 2011.

[16] Dimitrakopoulos, E. G., DeJong, M. J., Revisiting the rocking block: closed-form solutions and similarity laws. *Proceedings of the Royal Society A: Mathematical, Physical and Engineering Science*, **468**(2144), 2294–2318, 2012.

[17] Dimitrakopoulos, E. G., DeJong, M. J., Overturning of retrofitted rocking structures under pulse-type excitations. *Journal of Engineering Mechanics*, **138**(8), 963–972, 2012.

[18] Dimitrakopoulos, E. G., Nonsmooth analysis of the impact between successive skew bridge-segments. *Nonlinear Dynamics*, **74**(4), 911–928, 2013.

[19] Dimitrakopoulos, E. G., Giouvanidis, A. I., Seismic response analysis of the planar rocking frame. *Journal of Engineering Mechanics*, **141**(7), 04015003, 2015.

[20] Dimitrakopoulos, E. G., Paraskeva, T. S., Dimensionless fragility curves for rocking response to near-fault excitations. *Earthquake Engineering & Structural Dynamics*, **44**(12), 2015-2033, 2015.

[21] Dimitrakopoulos, E. G., Fung, E. D. W., Closed-form rocking overturning conditions for a family of pulse ground motions. *Proceedings of the Royal Society A: Mathematical, Physical and Engineering Science*, **472**(2196), 20160662, 2016.

[22] Giouvanidis, A. I., Dimitrakopoulos, E. G., Seismic analysis of hybrid rocking bridge bents. *Proceedings of the 2nd European Conference on Earthquake Engineering and Seismology*, Paper No 2251, Istanbul, Turkey, 2014.

[23] Giouvanidis, A. I., Dimitrakopoulos, E. G., Nonsmooth dynamic analysis of sticking impacts in rocking structures. *Bulletin of Earthquake Engineering*, **15**(3), 2273-2304, 2017.

[24] Giouvanidis, A. I., Dimitrakopoulos, E. G., Seismic reliability assessment of rocking bridge bents with flag-shaped hysteretic behavior. *Proceedings of the 16th World Conference on Earthquake Engineering*, Paper No 1259, Santiago, Chile, 2017.

[25] Giouvanidis, A. I., Dimitrakopoulos, E. G., Seismic performance of rocking frames with flag-shaped hysteretic behavior. *Journal of Engineering Mechanics*, **143**(5), 04017008, 2017.

[26] Glocker, C., *Set-valued force laws: dynamics of non-smooth systems*. Springer, 2001.

[27] Housner, G. W., The behavior of inverted pendulum structures during earthquakes. *Bulletin of the Seismological Society of America*, **53**(2), 403–417, 1963.

[28] Leine, R. I., Van Campen, D. H., Glocker, C. H., Nonlinear dynamics and modeling of various wooden toys with impact and friction. *Journal of Vibration and Control*, **9**(1-2), 25–78, 2003.

[29] Lemke, C. E., Bimatrix equilibrium points and mathematical programming. *Management Science*, **11**(7), 681–689, 1965.

[30] Lipscombe, P. R., Pellegrino, S., Free rocking of prismatic blocks. *Journal of Engineering Mechanics*, **119**(7), 1387–1410, 1993.

[31] Makris, N., Vassiliou, M. F., Planar rocking response and stability analysis of an array of free-standing columns capped with a freely supported rigid beam. *Earthquake Engineering & Structural Dynamics*, **42**(3), 431–449, 2012.

[32] Oliveto, G., Calio, I., Greco, A., Large displacement behaviour of a structural model with foundation uplift under impulsive and earthquake excitations. *Earthquake Engineering & Structural Dynamics*, **32**(3), 369–393, 2003.

[33] Payr, M., Glocker, C., Oblique frictional impact of a bar: analysis and comparison of different impact laws. *Nonlinear Dynamics*, **41**(4), 361–383, 2005.

[34] Pfeiffer, F., Glocker, C., *Multibody dynamics with unilateral contacts*. Springer Science & Business Media, 2000.

[35] Psycharis, I. N., Effect of base uplift on dynamic response of SDOF structures. *Journal of Structural Engineering*, **117**(3), 733–754, 1991.

[36] Psycharis, I. N., Fragiadakis, M., Stefanou, I., Seismic reliability assessment of classical columns subjected to near-fault ground motions. *Earthquake Engineering & Structural Dynamics*, **42**(14), 2061–2079, 2013.

[37] Shenton III, H. W., Jones, N., P., Base excitation of rigid bodies. I: Formulation. *Journal of Engineering Mechanics*, **117**(10), 2286–2306, 1991.

[38] Shi, Z., Dimitrakopoulos, E. G., Nonsmooth dynamics prediction of measured bridge response involving deck-abutment pounding. *Earthquake Engineering & Structural Dynamics*, **doi:10.1002/eqe.2863**, 2017.

[39] Truniger, R., Vassiliou, M. F., Stojadinovic B., An analytical model of a deformable cantilever structure rocking on a rigid surface: experimental validation. *Earthquake Engineering & Structural Dynamics*, **44**(15), 2795–2815, 2015.

[40] Vassiliou, M. F., Mackie, K. R., Stojadinovic B., Dynamic response analysis of solitary flexible rocking bodies: modeling and behavior under pulse-like ground excitation. *Earthquake Engineering & Structural Dynamics*, **43**(10), 1463–1481, 2014.

[41] Vassiliou, M. F., Truniger, R., Stojadinovic B., An analytical model of a deformable cantilever structure rocking on a rigid surface: development and verification. *Earthquake Engineering & Structural Dynamics*, **44**(15), 2775–2794, 2015.

[42] Vassiliou, M. F., Mackie, K. R., Stojadinovic B., A finite element model for seismic response analysis of deformable rocking frames. *Earthquake Engineering & Structural Dynamics*, **46**(3), 447-466, 2016.

[43] Vassiliou, M. F., Burger, S., Egger, M., Bachmann, J. A., Broccardo, M., Stojadinović, B., The three-dimensional behavior of inverted pendulum cylindrical structures during earthquakes. *Earthquake Engineering & Structural Dynamics*, **doi:10.1002/eqe.2903**, 2017.

[44] Yilmaz, C., Gharib, M., Hurmuzlu, Y., Solving frictionless rocking block problem with multiple impacts. *Proceedings of the Royal Society A: Mathematical, Physical and Engineering Science*, **doi:10.1098/rspa.2009.0273**, 2009.